Rich magnetic phase diagram of the kagome-staircase compound $Mn_3V_2O_8$

E. Morosan,[1] J. Fleitman,[1] T. Klimczuk,[2,3] and R. J. Cava[1]
[1]*Department of Chemistry, Princeton University, Princeton, New Jersey 08544, USA*
[2]*Division of Thermal Physics, Los Alamos National Laboratories, Los Alamos, New Mexico 87545, USA*
[3]*Faculty of Applied Physics and Mathematics, Gdansk University of Technology, Narutowicza 11/12, 80-952 Gdansk, Poland*
(Received 19 June 2007; published 1 October 2007)

We report the anisotropic magnetic phase diagrams for $Mn_3V_2O_8$, in which $S=5/2$ Mn^{2+} is found in the kagome-staircase lattice, based on magnetization and specific heat data. At low applied fields, the system first orders magnetically below $T_{m1}\approx 21$ K and then shows a second transition at $T_{m2}\approx 15$ K. In addition, a phase transition that is apparent in specific heat but not seen in magnetization is found for all field orientations, converging toward T_{m2} as $H\rightarrow 0$. The magnetic behavior is highly anisotropic, and the *H-T* phase diagrams are quite rich, with seven distinct phases observed.

DOI: 10.1103/PhysRevB.76.144403 PACS number(s): 75.30.Kz, 75.30.Gw

I. INTRODUCTION

Geometrically frustrated magnetic materials have recently emerged as the focus of intense study. Among these, compounds based on the kagome net, a regular planar lattice made from corner sharing of equilateral triangles, are of particular interest due to the very high degeneracy of energetically equivalent magnetic ground states. Breaking the ideal triangular symmetry of the kagome net typically favors one particular magnetically ordered state above others. For the particular case of the kagome-staircase geometry, however, in which the symmetry breaking occurs via buckling of the kagome plane (see inset to Fig. 1), an exquisitely close competition between different magnetically ordered states has been observed, resulting in complex temperature–applied field magnetic phase diagrams. The kagome-staircase lattice is observed in the transition metal vanadates $T_3V_2O_8$ (with T=Co, Ni, Cu, and Zn),[1–11] and the Ni (Refs. 2–4, 7, 8, and 11) and Co (Refs. 1–3, 5, and 6) variants have been widely studied. Simultaneous long-range ferroelectric and magnetic order have been found in $Ni_3V_2O_8$,[11] allowing its classification as a multiferroic compound.

Orthorhombic symmetry $Mn_3V_2O_8$ (MVO) is isostructural with $Co_3V_2O_8$ (CVO) and $Ni_3V_2O_8$ (NVO), but its physical properties have been only marginally studied.[12] The $t_{2g}^3e_g^2$, isotropic spin, $S=5/2$, $L=0$, configuration of Mn^{2+} in MVO presents an interesting contrast to the $t_{2g}^5e_g^2$ $S=3/2$ Co^{2+} and $t_{2g}^6e_g^2$ $S=1$ Ni^{2+} cases of CVO and NVO. Here, we report the observation of rich anisotropic magnetic field–temperature (*H-T*) phase diagrams for MVO, as determined from magnetization and specific heat measurements on single crystals. Magnetic phase transitions at 21 and 15 K are observed for fields applied in all three principal crystallographic directions. A phase transition that is apparent in specific heat but not seen in magnetization is found for all three applied field orientations, converging toward the 15 K transition as $H\rightarrow 0$. The critical fields for magnetic phase boundaries are much higher when the magnetic field is applied perpendicular to the kagome-staircase plane ($H\|b$) than when applied in plane ($H\|a$ or $H\|c$). The field-temperature (*H-T*) phase diagrams are quite rich, with seven distinct magnetic and/or structural phases observed. The magnetic phase diagrams are distinctly different from what is observed for CVO and NVO.

II. EXPERIMENTAL PROCEDURE

Single crystals of MVO were grown out of a $MoO_3/V_2O_5/MnO$ flux as previously described.[12] The starting oxides were packed in an alumina crucible, heated in a vertical tube furnace under flowing argon gas, with sacrificial MnO powder used to regulate the oxygen partial pressure.[12] The furnace was heated to 1200 °C at 200 °C/h, held at 1200 °C for 1 h, cooled to 900 °C at 5 °C/h, then cooled to room temperature at 300 °C/h. The red-brown platelet crystals were extracted from the flux using a bath of one part glacial acetic acid and three parts de-ionized water. The crystals were found to be single phase by single crystal and powder x-ray diffraction, with the orthorhombic *Cmca* structure and lattice parameters $a=6.2672(3)$ Å, $b=11.7377(8)$ Å, and $c=8.5044(5)$ Å. The magnetic Mn^{2+} ions form a buckled kagome plane, which is perpendicular to the crystallographic *b* direction (inset, Fig. 1). Field- and temperature-dependent

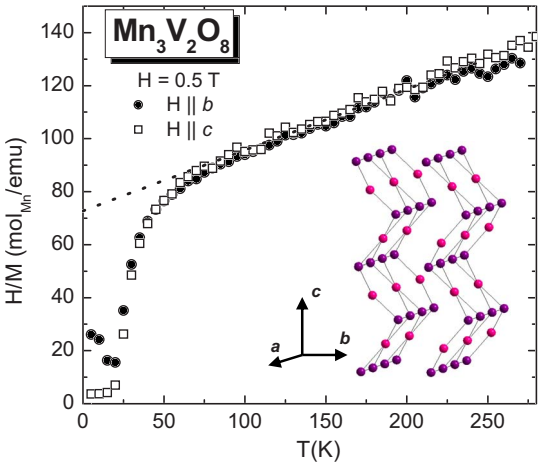

FIG. 1. (Color online) Anisotropic inverse susceptibility data for $H=0.5$ T (symbols) and linear fit of the high-temperature data (dotted line). Insert: kagome-staircase structure of the Mn^{2+} array in $Mn_3V_2O_8$.

magnetization and specific heat measurements were performed in a Quantum Design Physical Properties Measurement System (PPMS). A platelike single crystal with mass of 4.2 mg and dimension of $2\times1\times0.5$ mm^3 was used for all measurements.

III. RESULTS

The $H=0.5$ T inverse magnetization data for MVO (Fig. 1) indicate the presence of long-range magnetic ordering below $T_{m1}\approx21$ K. Previous low-field magnetization data[12] suggest the existence of an additional magnetic phase transition near 40 K, but that feature is most likely due to the presence of a $Mn_2V_2O_7$ impurity. A high-temperature fit of the susceptibility (dotted line, Fig. 1) to the Curie-Weiss law $\chi=\chi_0+C/(T-\theta_W)$ yields a temperature-independent susceptibility $\chi_0\approx-1.5\times10^{-3}$ emu/mol$_{Mn}$ and an effective moment $\mu_{eff}=5.94\mu_B$, in excellent agreement with the theoretical value $\mu_{eff}=5.92\mu_B$ expected for high-spin $S=5/2$ Mn^{2+}. The Weiss temperature $\theta_W=-320$ K indicates the dominance of antiferromagnetic exchange interactions. Given the kagome-staircase magnetic lattice (inset in Fig. 1), it is not surprising that $|\theta_W/T_{m1}|\approx15$, characteristic of a strongly frustrated antiferromagnetic spin system. Deviations from Curie-Weiss behavior are observed to begin on cooling at approximately 70 K.

The easy magnetization axis lies close to the crystallographic *ac* plane, where the magnetization is largest (Fig. 1). Upon further inspection, two magnetic phase transitions can be identified in the $M(T)$ data for all field orientations. Figure 2 illustrates the field dependence of these transitions for $H\|a$, $H\|b$, and $H\|c$, respectively. The competition between the antiferromagnetic spin coupling and the anisotropy associated with the kagome-staircase structure precludes the system from attaining a zero net magnetization ground state. This is suggested by the rapidly increasing magnetization as the system enters the high-temperature, low-field state (HT1) upon cooling below $T_{m1}\approx21$ K. A net ferromagnetic component can probably be associated with the HT1 phase. Subsequent cooling of the sample gives rise to a sharp cusp followed by a local minimum around $T_{m2}=15$ K, where a second magnetic phase transition, from HT1 to a low-T, low-H state (LT1) occurs. Increasing magnetic field (Fig. 2) has almost no effect on the long-range magnetic ordering temperature T_{m1}, but it broadens the cusp and slowly drives the second transition down in temperature. Above $H=0.04$ T, the $H\|a$ low-temperature magnetization plateaus at a finite value, which strongly suggests a canted spin configuration even for the LT1 state, with a smaller ferromagnetic component along a than in the HT1 state. Very similar behavior occurs for the other in-plane orientation $H\|c$ [Fig. 2(c)], with the two distinct transitions persisting up to a slightly higher field $H=0.1$ T. For $H\|b$ [Fig. 2(b)], two transitions are distinguishable up to an even higher field value $H=2.0$ T. The inset in Fig. 2(a) represents an example of how the critical temperatures for the magnetic phase transitions at constant field are determined: as shown, the vertical arrows mark T_{m1} and T_{m2}, $H=0.01$ T, and correspond to local minima in the temperature derivative of magnetization dM/dT. The two

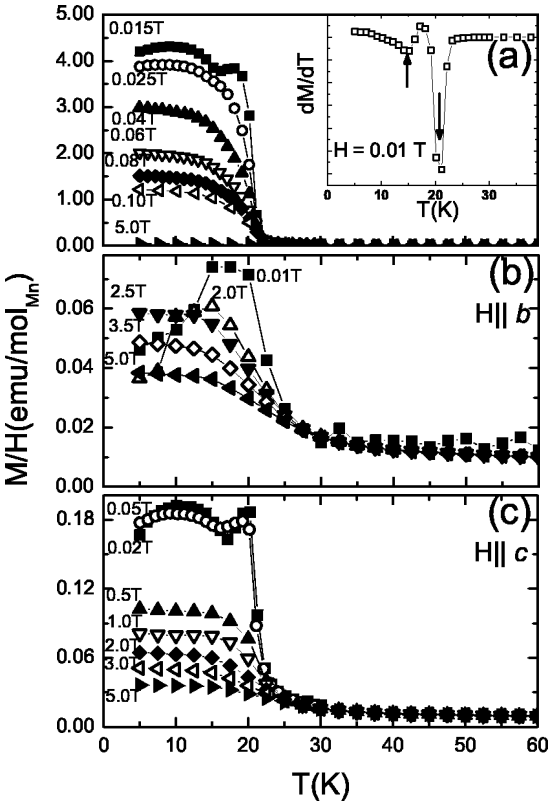

FIG. 2. $Mn_3V_2O_8$ $M(T)$ data for (a) $H\|a$, (b) $H\|b$, and (c) $H\|c$. Inset: the $H=0.01$ T dM/dT curve.

low-field phases that are observed in the magnetically ordered state are possibly a result of the ordering of the spins on one or both of the distinct Mn^{2+} ions (inset Fig. 1) in the *ac* plane, similar to the transitions encountered in NVO.[4] Fewer magnetic phases are distinguishable at low fields in MVO, however, than are seen in either NVO or CVO.

A more complex scenario is revealed in MVO at finite fields. Figure 3 shows a selection of the $M(H)$ isotherms (left axis), with the $T=2$ K $H\|b$ field derivative dM/dH (crosses) as an example of how the critical field values were determined. When $H\|a$ [Fig. 3(a)], the $T=2$ K magnetization rapidly increases with H at low-field values, consistent with a large ferromagnetic component of the magnetization in this direction. For $H\|b$ [Fig. 3(b)], the $T=2$ K magnetization is low and linear with field for $H<2$ T, which corresponds to the LT1 phase. This behavior is consistent with the antiferromagnetic spins slowly rotating from the easy axis in the ac plane, closer to the direction of the applied field $H\|b$. A sharp step in magnetization around $H_{c1}=2.1$ T marks the transition from LT1 to LT2. The magnetization increases linearly with field above H_{c1} and another transition occurs just below 3 T, where $M(H)$ changes slope [open squares, Fig. 3(b)] and the system enters the state LT3. The H_{c1} transition yields a sharp peak in dM/dH [crosses, right axis Fig. 3(b)]; the higher critical field value H_{c2} is determined using an onset criterion for dM/dH. Both transitions are marked by small vertical arrows in Fig. 3(b). Similar to the other in-plane field orientation, the $H\|c$ magnetization [Fig. 3(c)] rapidly increases at low fields; as H becomes higher than

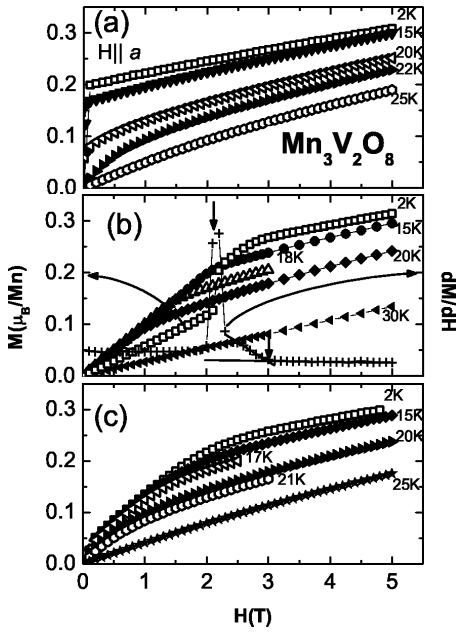

FIG. 3. $Mn_3V_2O_8$ $M(H)$ isotherms for (a) $H\|a$, (b) $H\|b$, and (c) $H\|c$ (left axis) and the $H\|bT=2$ K dM/dH curve [crosses, right axis (b)].

0.3 T, the LT1 to LT2 transition is evidenced by the change in slope of the $T=2$ K $M(H)$ curve. Upon further increasing the applied field, a transition from LT2 to LT3 occurs, similar to that for $H\|b$.

As the temperature is raised, the initial increase of the magnetization for $H\|a$ becomes smaller and smaller, and above 22 K the $M(H)$ curves become almost linear in field, consistent with the system entering the paramagnetic state above $T_{m1}\approx 21$ K. For $H\|b$, the initial slope of the $M(H)$ curves increases in the magnetically ordered phase [Fig. 3(b)] such that the magnetization jump at the LT1 to LT2 transition becomes indistinguishable. The two magnetic phase transitions move slightly down with field and are hard to identify in the magnetization measurements above 16 K. In a similar manner, the two transitions are visible in the $H\|c$ direction [Fig. 3(c)] only up to $T=17$ K.

Specific heat measurements complement the magnetization data not only by confirming the magnetic phase lines but also by revealing another phase transition that was not visible in the $M(T,H)$ data. A selection of the specific heat curves, plotted as C_p/T vs T, is shown in Fig. 4(a), for $H\|b$ and applied fields up to 9 T. For $H=0$ (full squares), a sharp peak associated with long-range magnetic ordering is seen around $T_{m1}=21$ K, with a second peak at the lower phase transition temperature T_{m2}. In order to estimate the magnetic contribution to the specific heat of MVO, the specific heat of the nonmagnetic analogous compound $Zn_3V_2O_8$ (ZVO)[2] was measured. Using a renormalization ratio $\rho_{\text{ren}}=(M_{\text{MVO}}/M_{\text{ZVO}})^{1/2}$,[13] where M_{MVO} and M_{ZVO} are the molecular weights of MVO and ZVO, respectively, the lattice contribution to the specific heat was calculated according to the Debye model. This was subtracted from the specific heat of MVO to give the magnetic contribution C_m(MVO) [open symbols, Fig. 4(b)]. The temperature dependence of the magnetic entropy can then be calculated and is shown in the inset in Fig. 4(b) for $H=0$ (open circles): only about 50% of the $R\ln 6$ entropy expected for an $S=5/2$ state is accounted for between 2 and 40 K. This could indicate that additional phase transitions may exist below 2 K or that more entropy is associated with short-range order below 70 K. Further work is required to explore the temperature dependence of the entropy above and below the temperature range of the current study. No additional entropy is recovered with the application of magnetic field, as the $H=9$ T temperature-dependent entropy [crosses, inset Fig. 4(b)] differs only slightly from the $H=0$ data. However, as the field is turned

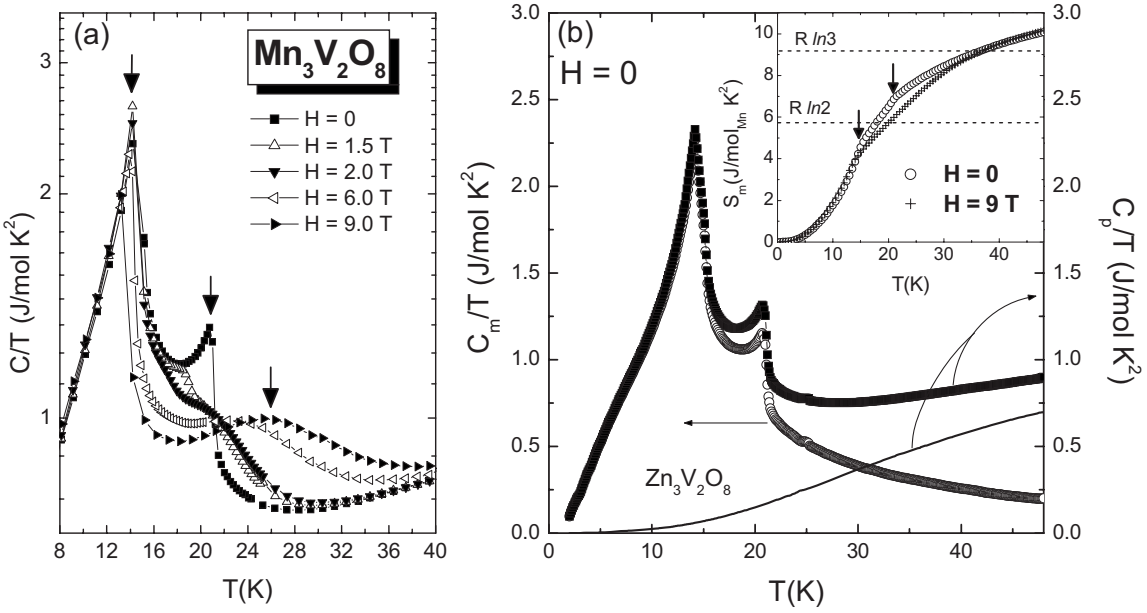

FIG. 4. (a) MVO $H\|b$ C_p/T vs T data. (b) C_p/T data for MVO (full symbols) and $Zn_3V_2O_8$ (solid line) (right axis), together with the magnetic specific heat C_m/T of MVO (open symbols, left axis). Inset: the magnetic entropy S_m for $H=0$ and 9 T.

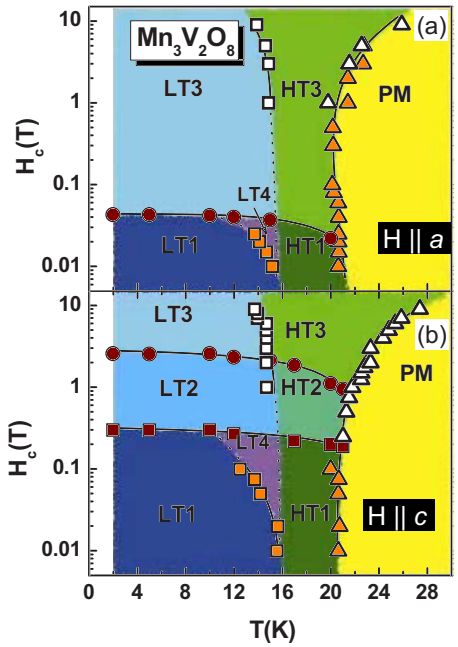

FIG. 5. (Color online) (a) $H\|a$ and (b) $H\|c$ H-T phase diagrams: points are determined from $M(T)$ data (orange symbols), $M(H)$ data (wine symbols), or $C_p(T)_{|H}$ data (open symbols). The solid lines are guides connecting the points determined experimentally; extrapolations of these phase boundaries in regions where measurements were missing or critical H and T values were difficult to determine are represented by dotted lines.

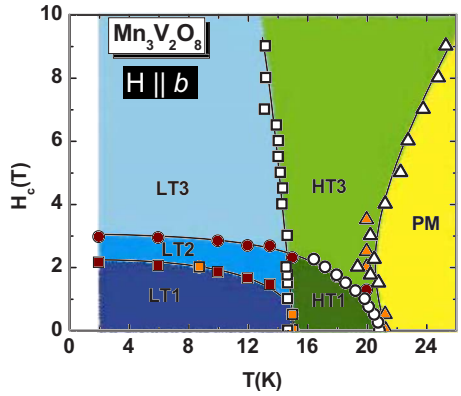

FIG. 6. (Color online) $H\|b$ H-T phase diagrams: points are determined from $M(T)$ data (orange symbols), $M(H)$ data (wine symbols), or $C_p(T)_{|H}$ data (open symbols). The solid lines are guides connecting the points determined experimentally; extrapolations of these phase boundaries in regions where measurements were missing or critical H and T values were difficult to determine are represented by dotted lines.

on, a very different behavior is observed for the two peaks in C_p [Fig. 4(a)]: the one just below 16 K is affected little in temperature by the increasing magnetic field, but the higher-temperature one moves down in field. Concurrently, a third, broader peak emerges above ~1.5 T and is driven higher in temperature with increasing field. It is likely that both phase transitions exist at finite fields even for $H<1.5$ T and converge at T_{m1} for $H\rightarrow 0$, but their proximity in temperature makes it impossible to discern two separate peaks. For $H>H^b_{c1}$, the lower temperature peak is not associated with any phase transition observed in the magnetization data. Given its invisibility in the magnetization and the relative insensitivity of the transition temperature to applied field, we speculate that this transition may have a structural component, though the fact that the amount of entropy in the transition is suppressed by the field indicates that there must be a magnetic component as well.

Our experimentally determined H-T magnetic phase diagrams for MVO, for magnetic fields applied along the unique structural directions, are presented in Figs. 5 and 6. As the temperature is lowered in zero field, MVO orders magnetically at $T_{m1}=20.7\pm0.2$ K, entering first a high-temperature phase (HT1) and then a low-temperature phase (LT1) at $T_{m2}=15.2\pm0.5$ K. The response of the system to the applied magnetic field is highly anisotropic. For $H\|a$ [Fig. 5(a)], in finite field, two distinct phase boundaries emerge at T_{m2}: one represents the lower temperature magnetic phase transition, which moves down in temperature as H increases, and the second is an almost vertical line, which is only visible in the specific heat data. The intermediate temperature phase delineated by these two phase boundaries is LT4, which extends in field up to about 0.04 T. An almost horizontal phase line cuts across the phase diagram at $H^a_{c1}\approx 0.04$ T. It separates the low-field, low-temperature (LT1) and high-temperature (HT1) phases from two different states (LT3 and HT3) at higher fields.

For the other field orientation close to the plane [$H\|c$, Fig. 5(b)], the low-field phase diagram is similar to that for $H\|a$, with the HT1, LT4, and LT1 phases extending up in field up to a much higher critical value $H^c_{c1}=0.3$ T. In the $T\rightarrow 0$ limit, a second magnetic phase transition occurs at $H^c_{c2}=2.6$ T, and the critical field value is slowly reduced with temperature. The two almost horizontal phase lines at H^c_{c1} and H^c_{c2} separate a low-temperature (LT2) and a high-temperature (HT2) phase at intermediate field values from the high field states LT3 and HT3.

When field is applied perpendicular to the kagome planes (Fig. 6), the phase diagram is analogous to the in-plane ones. The most noticeable difference is that the critical field values are much higher: $H^b_{c1}=2.2$ T and $H^b_{c2}=3.0$ T for $T\rightarrow 0$. This is expected given the observed anisotropy, which constrains the magnetic moments to lie closer to the ac plane: stronger fields are needed to pull the moments toward the "hard" axis b. In addition, the LT4 phase is missing, and the phase line that starts at H^b_{c1} at $T\rightarrow 0$ converges at T_{m2} in the $H=0$ limit. As a consequence, the HT2 phase merges with HT1 just below the magnetic ordering at T_{m1}.

IV. CONCLUSIONS

The temperature-field magnetic phase diagram for $Mn_3V_2O_8$ is quite different from those seen in $Ni_3V_2O_8$ and $Co_3V_2O_8$. In all three compounds, the competition between the crystalline anisotropy and the antiferromagnetic interactions in the kagome-staircase structure gives rise to the strong geometric frustration. In NVO and CVO, differences in the magnetically ordered states have been found to involve

differences in the ordering of the moments on the two kinds of magnetic ion sites, the so-called spine and crosstie sites. The same will no doubt prove true for MVO, with the present measurements revealing that the magnetic moments on the two distinct Mn^{2+} sites lie close to the *ac* plane when in the $H=0$ magnetically ordered states. For magnetic fields applied in plane, the magnetic states in MVO are much more sensitive to the applied field than they are in NVO and CVO, with Fig. 5 showing for example that the LT1 and HT1 phases disappear in applied fields in the *a* direction as low as 0.04 T. The complexity of the anisotropic *H-T* phase diagrams in MVO appears to be derived from the competition between nearly balanced magnetic interactions, leading to canted spin configurations. An integration of the entropy observed under the $H=0$ phase transitions between 2 and 40 K does not yield the expected $R \ln 6$ for Mn^{2+}, suggesting that there may be more magnetic phase transitions below 2 K or that additional entropy is associated with short-range order below 70 K. Detailed neutron scattering measurements are desirable in order to elucidate the nature of the different states observed in MVO and also to clarify whether the almost field independent phase boundary at T_{m2} is associated with a structural phase transition. Investigation of possible multiferroic phases will also be of considerable interest.

ACKNOWLEDGMENTS

This research was supported by the U.S. Department of Energy, Division of Basic Energy Sciences, Grant No. DE-FG02- 98-ER45706. We thank G. Lawes for providing the specific heat data for $Zn_3V_2O_8$.

[1] N. Krishnamachari, and C. Calvo, Can. J. Chem. **49**, 1629 (1971).
[2] N. Rogado, G. Lawes, D. A. Huse, A. P. Ramirez, and R. J. Cava, Solid State Commun. **124**, 229 (2002).
[3] G. Balakrishnan, O. A. Petrenko, M. R. Lees, and D. McK Paul, J. Phys.: Condens. Matter **16**, L347 (2004).
[4] M. Kenzelmann, A. B. Harris, A. Aharony, O. Entin-Wohlman, T. Yildirim, Q. Huang, S. Park, G. Lawes, C. Broholm, N. Rogado, R. J. Cava, K. H. Kim, G. Jorge, and A. P. Ramirez, Phys. Rev. B **74**, 014429 (2006).
[5] R. Szymczak, M. Baran, R. Diduszko, J. Fink-Finowicki, M. Gutowska, A. Szewczyk, and H. Szymczak, Phys. Rev. B **73**, 094425 (2006).
[6] Y. Chen, J. W. Lynn, Q. Huang, F. M. Woodward, T. Yildirim, G. Lawes, A. P. Ramirez, N. Rogado, R. J. Cava, A. Aharony, O. Entin-Wohlman, and A. B. Harris, Phys. Rev. B **74**, 014430 (2006).
[7] R. P. Chaudhury, F. Yen, C. R. dela Cruz, B. Lorenz, Y. Q. Wang, Y. Y. Sun, and C. W. Chu, Phys. Rev. B **75**, 012407 (2007).
[8] G. Lawes, M. Kenzelmann, N. Rogado, K. H. Kim, G. A. Jorge, R. J. Cava, A. Aharony, O. Entin-Wohlman, A. B. Harris, T. Yildirim, Q. Z. Huang, S. Park, C. Broholm, and A. P. Ramirez, Phys. Rev. Lett. **93**, 247201 (2004).
[9] N. Rogado, M. K. Haas, G. Lawes, D. A. Huse, A. P. Ramirez, and R. J. Cava, J. Phys.: Condens. Matter **15**, 907 (2003).
[10] E. E. Sauerbrei, R. Faggiani, and C. Calvo, Acta Crystallogr., Sect. B: Struct. Crystallogr. Cryst. Chem. **29**, 2304 (1973).
[11] G. Lawes, A. B. Harris, T. Kimura, N. Rogado, R. J. Cava, A. Aharony, O. Entin-Wohlman, T. Yildrim, M. Kenzelmann, C. Broholm, and A. P. Ramirez, Phys. Rev. Lett. **95**, 087205 (2005).
[12] X. Wang, Z. Liu, A. Ambrosini, A. Maignan, C. L. Stern, K. R. Poeppelmeier, and V. P. Dravid, Solid State Sci. **2**, 99 (2000).
[13] A. A. Azhar, C. D. Mitescu, and W. R. Johanson, J. Appl. Phys. **57**, 3235 (1985).